SLAC–PUB–5718 Rev.
DAPNIA/SPP 92–02
April 1992
(T/E/A)

Beamstrahlung Spectra in Next Generation Linear Colliders

T. Barklow and P. Chen
Stanford Linear Accelerator Center
Stanford University, Stanford, Ca 94309
and
W. Kozanecki
DAPNIA-SPP, CEN-Saclay
F91191 Gif-sur-Yvette (France)

Abstract: For the next generation of linear colliders, the energy loss due to *beamstrahlung* during the collision of the e^+e^- beams is expected to substantially influence the effective center-of-mass energy distribution of the colliding particles. In this paper, we first derive analytical formulae for the electron and photon energy spectra under multiple beamstrahlung processes, and for the e^+e^- and $\gamma\gamma$ differential luminosities. We then apply our formalism to various classes of 500 GeV e^+e^- linear collider designs currently under study.

Contributed to the ECFA Workshop on Physics With Linear Colliders, Hamburg, Germany, September 2–3, 1991

---

*Work supported by Department of Energy contract DE–AC03–76SF00515.

1 Introduction

In future Linear Colliders, contrarily to what happens in storage rings such as LEP, the e^+e^- center-of-mass (c.m.) energy is no longer confined to twice the primary beam energy, but instead gets spread over a relatively wide distribution, due to the onset of *beamstrahlung* [1], the synchrotron radiation emitted by one of the colliding bunches in the field of the opposing one. The energy so radiated by the beam particles spans a range that extends, depending on the accelerator design, from a few per mil to several tens of percent of the nominal electron energy E_0. Realistic simulation of physics processes whose cross-section or kinematics are energy-dependent (such as the top threshold scan), therefore mandates an accurate description of the differential luminosity as a function of the effective c.m. energy. In addition, the low energy end of the e^{+-} and γ spectra are also important to understand the implications of accelerator-induced backgrounds and of high energy photon-photon scattering processes.

When the average number of beamstrahlung photons radiated per beam particle is much less than unity, the energy spectrum for the final e^+ or e^- beam is simply the well-known Sokolov-Ternov spectrum [2] for the radiated photons, with the fractional photon energy, $y(\equiv E_\gamma/E_0)$, replaced by the corresponding final electron (or positron) energy, $x = 1 - y$. When conditions are such that the average number of photons radiated is not much less than unity, the effect of successive radiation processes becomes important. Previously, the multiphoton beamstrahlung process has been studied by Blankenbecler and Drell [3], and independently by Yokoya and Chen [4]. More recently, Chen [5] derived, for the multiphoton beamstrahlung process, the electron and photon energy and luminosity spectra. In this paper, we adopt the formulae derived in ref. [5] and investigate the electron and photon energy and luminosity spectra for several Linear Collider designs. We first review in section 2 the electron and the photon spectra under multiphoton beamstrahlung, and derive the e^+e^- and $\gamma\gamma$ differential luminosity functions. Section 3 sketches the broad classes of Linear Collider concepts currently under consideration, and fixes, for each class, a set of representative interaction point (IP) parameters. In Section 4 we apply our formalism to the computation of typical electron and photon energy and luminosity spectra for these five collider designs. Our findings are summarized in the last section.

2 Multiphoton Beamstrahlung Spectra

In this section we review the analytic derivation of electron and photon energy and luminosity spectra under multiphoton beamstrahlung process. Mathematical details of the derivation can be found in ref. [5].

Let $\psi(x,t)$ be the energy spectral function of the electron for energy $x \equiv E/E_0$ at time t normalized as $\int \psi(x,t)dx = 1$. We assume that the emission of the photon takes place in an infinitesimally short time interval. Then the interference between two successive

emissions is negligible, and the evolution of the spectral function can be described by the rate equation

$$\frac{\partial \psi}{\partial t} = -\nu(x)\psi(x,t) + \int_x^1 dx' F(x,x')\psi(x',t) \quad . \tag{1}$$

Here $\nu(x)$ is the average number of photons radiated per unit time and F is the spectral function of radiation, i.e., $F(x,x')dx'$ is the transition probability of an electron from energy x' to the energy interval $(x, x+dx)$ per unit time.

The spectral function of radiation can be characterized by the beamstrahlung parameter Υ, defined as

$$\Upsilon = \gamma_0 \frac{B}{B_c} \quad , \tag{2}$$

where $\gamma_0 = E_0/mc^2$, B is the effective field strength in the beam, and $B_c = m^2c^3/e\hbar \sim 4.4 \times 10^{13}$ Gauss is the Schwinger critical field. High energy e^+e^- beams generally follow Gaussian distributions in the three spatial dimensions. Thus the local field strength varies inside the beam volume. It can be shown, however, through integrating over the impact parameter and the longitudinal variations, that the overall beamstrahlung effect can be simply described as if all particles experience a *mean field*

$$\Upsilon_{mean} \simeq \frac{5}{6} \frac{r_e^2 \gamma_0 N}{\alpha \sigma_z (\sigma_x + \sigma_y)} \quad , \tag{3}$$

where r_e is the classical electron radius, α the fine structure constant, N the total number of particles in a bunch, and $\sigma_x, \sigma_y, \sigma_z$ are the sizes of the beam. We shall thus take $\Upsilon \equiv \Upsilon_{mean}$ for the entire beam.

The effective beam sizes which one uses in calculating Υ_{mean} are in general different from the nominal beam sizes because the "disruption" effect tends to deform the beams during collision. This is especially true of the horizontal beam size σ_x in the flat beam machine designs we consider in this paper. Define the horizontal disruption parameter D_x as

$$D_x = \frac{2Nr_e\sigma_z}{\gamma\sigma_x(\sigma_x + \sigma_y)} \quad . \tag{4}$$

The effective σ_x can be deduced from the luminosity enhancement factor H_D, defined as [6]

$$H_D = 1 + \frac{2}{3\sqrt{\pi}} D_x \quad , \quad D_x \ll 1 \quad . \tag{5}$$

Since the enhancement results from the reduction of the effective beam size, we can estimate the effective σ_x as

$$\bar{\sigma}_x \sim \frac{\sigma_x}{\sqrt{H_D}} \quad . \tag{6}$$

We then substitute $\bar{\sigma}_x$ for σ_x in Eq.(3) when calculating Υ_{mean}.

By definition,

$$\nu(x) = \int_0^x F(x',x)dx' \equiv \nu_{cl} U_0(x\Upsilon) \quad , \tag{7}$$

where ν_{cl} is the number of photons per unit time, (or length, with $c = 1$) calculated by the classical theory of radiation,

$$\nu_{cl} = \frac{5}{2\sqrt{3}} \frac{\alpha^2}{r_e \gamma_0} \Upsilon \quad . \tag{8}$$

Note that for a given field strength ν_{cl} is independent of the particle energy. The function $U_0(v)$ is normalized such that $U_0(0) = 1$, and can be represented by the following approximate expression:

$$\begin{aligned} U_0(v) \quad &= \begin{cases} 1 \quad , & v \to 0 \quad , \\ (28\sqrt{3}/45)\Gamma(2/3)(3v)^{-1/3} = 1.012 v^{-1/3}, & v \to \infty \quad , \end{cases} \\ &\approx [1 + v^{2/3}]^{-1/2} \quad . \end{aligned} \tag{9}$$

To look for a compact analytic solution for ψ in Eq.(1), we invoke an approximate expression for $F(x, x')$,

$$F(x, x') = \frac{1}{\Gamma(1/3)} \frac{\nu_{cl}\kappa}{x x'} \eta^{-2/3} e^{-\eta} \quad , \tag{10}$$

where $\kappa \equiv 2/(3\Upsilon)$ and $\eta = \kappa[(1/x) - (1/x')]$. The solution is

$$\psi(x, t) = e^{-\nu_{cl} t} \Big[\delta(1 - x) + \frac{e^{-\eta_x}}{1 - x} h(\eta_x^{1/3} \nu_{cl} t) \Big] \quad . \quad \Upsilon \ll 1 \quad , \tag{11}$$

where $\eta_x \equiv \kappa[(1/x) - 1]$, and

$$h(u) = \frac{1}{2\pi i} \int_{\lambda - i\infty}^{\lambda + i\infty} \exp(u p^{-1/3} + p) dp = \sum_{n=1}^{\infty} \frac{u^n}{n! \Gamma(n/3)} \quad , \tag{12}$$

with $\lambda > 0$ and $0 \le u \le \infty$. The first term in Eq.(11) represents the electron population that suffers no radiation. The n^{th} term in the Taylor expansion of the second term corresponds to the process of n-photon emissions.

For finite values of Υ, the rate equation cannot be solved exactly since $\nu(x)$ is not constant in time any more. However, in the intermediate regime where $\Upsilon \lesssim \mathcal{O}(10)$, $\nu(x)$ should not deviate from ν_{cl} too significantly. This suggests a solution based upon minor perturbation from the above classical result. It is found [4] that

$$\psi(x, t) = e^{-\nu_\gamma t} \Big[\delta(1 - x) + \frac{e^{-\eta_x}}{1 - x} h(\eta_x^{1/3} \bar{\nu} t) \Big] \quad , \quad \Upsilon \lesssim 10 \quad , \tag{13}$$

for the intermediate regime, where

$$\nu_\gamma \equiv \nu(x = 1) = U_0(\Upsilon) \nu_{cl} \quad , \qquad \bar{\nu} \equiv x \nu_{cl} + (1 - x) \nu_\gamma \quad . \tag{14}$$

In effect, $\bar{\nu}$ is a linear interpolation between the two extrema ν_{cl} and ν_γ. We see that $\bar{\nu} \to \nu_{cl}$ as $x \to 1$, since for the electron to remain at high energy after n-photon process, it can only have radiated classically. On the other hand, $\bar{\nu} \to \nu_\gamma$ as $x \to 0$. This indicates that the low–energy end of the electron spectrum is dominated by quantum radiation.

Next we look for the companion formulas for the beamstrahlung photons. Let us ignore the loss of photons due to beamstrahlung pair creation [7], which constitutes only

a fraction $\sim \alpha$ (fine structure constant) of the total photon population. Then the time evolution of the spectrum is dominated by the beamstrahlung process alone:

$$\frac{\partial \phi}{\partial t} = \int_y^1 dx F(x-y,x)\psi(x,t) \quad , \tag{15}$$

where $y \equiv E_\gamma / E_0$ is the photon fractional energy. Therefore

$$\phi(y,t) = \int_0^t dt' \int_y^1 dx F(x-y,x)\psi(x,t') \quad . \tag{16}$$

Note that while $\int \psi(x,t)dx = 1$, which conserves the electron (or positron) number, the photon number cumulates along the course of collision, and in general $\int \phi(y,t)dy \neq 1$.

The solution of Eq.(16) is found [1] to be

$$\phi(y,t) = \frac{\kappa^{1/3}}{\Gamma(1/3)} y^{-2/3}(1-y)^{-1/3} e^{-\kappa y/(1-y)} G(y) \quad , \quad \Upsilon \ll 1, \tag{17}$$

where

$$\begin{aligned} G(y) &= \tfrac{1}{g(y)}\left[1 - e^{-g(y)\nu_{cl}t}\right] \quad , \\ g(y) &= 1-(1-y)^{2/3} \quad . \end{aligned} \tag{18}$$

Note that in the limit $\nu_{cl}t \ll 1$, the terms in the bracket can be replaced by $g(y)\nu_{cl}t$. This recovers the known expression for the beamstrahlung photon spectrum using single-photon (i.e., disregarding the loss of e^- energy between successive radiation processes) picture:

$$\lim_{\nu_{cl}t \to 0} \phi(y,t) = \frac{\kappa^{1/3}}{\Gamma(1/3)} y^{-2/3}(1-y)^{-1/3} e^{-\kappa y/(1-y)} \nu_{cl} t \quad . \tag{19}$$

In the $y \ll 1$ limit, the y dependence is approximately $\propto y^{-2/3}$.

To extend our result to the non-classical regime, we follow the same philosophy as in the case of electron spectrum by adopting the same general expression from the classical limit and introduce an average photon number per unit time over the entire spectrum:

$$\langle \bar{\nu} \rangle = \frac{1}{1-y}\int_y^1 dx[x\nu_{cl} + (1-x)\nu_\gamma] = \frac{1}{2}\left[(1+y)\nu_{cl} + (1-y)\nu_\gamma\right] \quad . \tag{20}$$

After some mathematical details, one eventually obtains

$$\phi(y,t) = \frac{\kappa^{1/3}}{\Gamma(1/3)} y^{-2/3}(1-y)^{-1/3} e^{-\kappa y/(1-y)} \tilde{G}(y) \quad , \quad \Upsilon \lesssim 5, \tag{21}$$

where

$$\begin{aligned} \tilde{G}(y) &= \frac{1-w}{\tilde{g}(y)}\left[1 - e^{-\tilde{g}(y)\nu_\gamma t}\right] + w\left[1 - e^{-\nu_\gamma t}\right] \quad , \\ \tilde{g}(y) &= 1 - \frac{\langle \bar{\nu} \rangle}{\nu_\gamma}(1-y)^{2/3} \quad ; \qquad w = \frac{1}{6\sqrt{\kappa}} \quad . \end{aligned} \tag{22}$$

This formula agrees quite well with the Monte Carlo simulation result. [5]

To find the differential luminosity $\mathcal{L}(s)$ as a function of the effective center-of-mass energy squared, s, one needs to convolute the energy spectrum of one beam, $\psi(x_1,t)$, with the other, $\psi(x_2,t)$. Let $t=0$ when the e^+e^- bunches first meet. Then the first z-slice in beam #1 will always encounter a "fresh" beam #2:

$$\frac{d\mathcal{L}_{e^+e^-}(0)}{dz} \propto \frac{2}{l}\int_0^{l/2} dt\psi(x_1,t)\psi(x_2,0) \quad , \tag{23}$$

where l is the total length of each bunch. For convenience of calculations, it is customary to consider uniform particle distribution in the longitudinal dimension. In that case, the effective bunch length is $l=2\sqrt{3}\sigma_z$, in relating to the Gaussian distribution. The total collision time is $l/2$ because both beams move with the speed of light against each other. A slice at z in beam #1, however, will always see a beam #2 which has evolved for a time $t=z/2$:

$$\frac{d\mathcal{L}_{e^+e^-}(z)}{dz} \propto \frac{2}{l}\int_0^{l/2} dt\psi(x_1,t)\psi(x_2,z/2) \quad . \tag{24}$$

Adding all z-slices in beam #1 together, we have

$$\begin{aligned}\mathcal{L}_{e^+e^-} &\propto \tfrac{4}{l^2}\int_0^{l/2} dt\psi(x_1,t)\int_0^{l} dz\psi(x_2,z/2) \\ &= \tfrac{4}{l^2}\int_0^{l/2} dt\psi(x_1,t)\int_0^{l/2} dz\psi(x_2,z) \quad .\end{aligned} \tag{25}$$

Note that the above two integrals are functionally identical. Inserting the spectral function in Eq.(12), we find, for $\Upsilon \ll 1$,

$$\begin{aligned}\psi(x) &\equiv \tfrac{2}{l}\int_0^{l/2} dt\psi(x,t) \\ &= \tfrac{1}{N_{cl}}\left[(1-e^{-N_{cl}})\delta(1-x)+\tfrac{e^{-\eta_x}}{1-x}\bar{h}(x)\right] \quad , \quad \Upsilon \ll 1 \quad ,\end{aligned} \tag{26}$$

where $\eta_x=\kappa[(1/x)-1]$, and $N_{cl}=\nu_{cl}l/2$ is the average number of photons radiated per particle during the entire collision of the e^+e^- beams. The function $\bar{h}(x)$ in the second term is

$$\bar{h}(x) = \sum_{n=1}^{\infty}\frac{\eta_x^{n/3}}{n!\Gamma(n/3)}\gamma(n+1,N_{cl}) \quad . \tag{27}$$

where $\gamma(n+1,N_{cl})$ is the incomplete gamma function.

The center-of-mass energy squared is $s \equiv x_1x_2$. The differential luminosity as a function of s is therefore

$$\mathcal{L}_{e^+e^-}(s) = \mathcal{L}_0\int_s^1\int_0^1 dx_1dx_2\delta(s-x_1x_2)\psi(x_1)\psi(x_2) \quad , \tag{28}$$

where $\mathcal{L}_0$ is the nominal luminosity of the collider, including the *enhancement factor* due to the beam-beam disruption effect [8].

The $\gamma\gamma$ center-of-mass luminosity can be obtained in much the same way. We find, for $\Upsilon \ll 1$,

$$\phi(y) = \frac{2}{l}\int_0^{l/2} dt\phi(y,t) = \frac{\kappa^{1/3}}{\Gamma(1/3)}y^{-2/3}(1-y)^{-1/3}e^{-\kappa y/(1-y)}\bar{G}(y) \quad , \tag{29}$$

where

$$\bar{G}(y) = \frac{1}{g(y)}\Big\{1 - \frac{1}{g(y)N_{cl}}\Big[1 - e^{-g(y)N_{cl}}\Big]\Big\} \quad . \tag{30}$$

For the non-classical regime, the corresponding expression reads

$$\phi(y) = \frac{\kappa^{1/3}}{\Gamma(1/3)} y^{-2/3}(1-y)^{-1/3} e^{-\kappa y/(1-y)} \bar{\tilde{G}}(y) \quad , \quad \Upsilon \lesssim 5, \tag{31}$$

where

$$\bar{\tilde{G}}(y) = \frac{1-w}{\tilde{g}(y)}\Big\{1 - \frac{1}{\tilde{g}(y)N_\gamma}\Big[1 - e^{-\tilde{g}(y)N_\gamma}\Big]\Big\} + w\Big\{1 - \frac{1}{N_\gamma}\Big[1 - e^{-N_\gamma}\Big]\Big\}. \tag{32}$$

The center-of-mass $\gamma\gamma$ luminosity is then

$$\mathcal{L}_{\gamma\gamma}(s) = \mathcal{L}_0 \int_s^1 \int_0^1 dy_1 dy_2 \delta(s - y_1 y_2)\phi(y_1)\phi(y_2) \quad . \tag{33}$$

Since the integration is quite involved, simple analytic expression of $L_{\gamma\gamma}$ for the whole range of $0 \leq s \leq 1$ is not easily attainable, and numerical calculations may be necessary.

3 Linear Collider Designs

Before presenting typical luminosity spectra, we must specify a consistent set of interaction point (IP) parameters, as the power spectrum of beamstrahlung is exceedingly sensitive to the strength of the oncoming electromagnetic field, i.e. to the charge density of the colliding bunches.

Optimization of a Linear Collider design, which involves a very large number of parameters subject to a dazzling network of constraints, has evolved into a fine art [9]. There currently exist many different approaches to building a 500 GeV c.m. energy Linear Collider, that fall into three broad classes [10,11] : SLAC and KEK propose a room-temperature, travelling-wave copper structure operating at 11.4 GHz (X-band), and a gradient of 50 to 100 MV/m [12]. About 10 bunches spaced 1 ns apart are accelerated within the 80 ns long machine pulse, yielding reasonable luminosity with low enough single bunch currents to keep beamstrahlung at an acceptably low level for most physics purposes (designs 1 and 2). DESY/Darmstadt suggest to extend the present SLC technology to higher energies [13,14], using a warm copper travelling-wave structure operating at 2.8 GHz and with a gradient of 17 MV/m. Energy extraction efficiency and luminosity are achieved by using as many as 172 bunches, spaced 11 ns apart, and accelerated within the 2.4 microsecond long R.F. pulse (designs 3 and 4). TESLA [15] proposes to use a superconducting standing wave RF structure at 1.3 GHz, with a gradient of 25 MV/m and a quality factor $Q_0 = 5 \times 10^9$. A total of 800 bunches spaced about 1 microsecond apart are accelerated within the 1.4 ms long RF pulse (design 5).

Of the many parameter sets available, we selected five, that hopefully span a fully representative range of accelerator concepts and philosophies. Their IP parameters, listed in Table 1, are only meant to be representative of each class; they should not be misconstrued as "official" parameters adopted by the designers themselves, as that work is still very much in flux.

Table 1: Summary of Interaction Point Linear Collider Parameters

Design Class	1 Palmer G	2 Palmer F	3 D-D wide bd	4 D-D nrrw bd	5 TESLA nrrw bd
Luminosity (10^{33} cm^{-2} s^{-1})	5.9	1.4	2.6	1.0	2.1
Bunches per pulse k_b	10	10	172	172	800
Bunch separation (ns)	1	1	11	11	900
Repetition rate f_{rep} (Hz)	130	130	50	50	10
Particles per bunch N (10^{10})	1.67	1.67	2.10	2.10	4.20
Horizontal spot size σ_x (nm)	166	612	316	632	1000
Vertical spot size σ_y (nm)	6.5	3.4	35	51	100
Bunch length σ_z (mm)	.110	.110	.400	1.0	2.0
Linac E spread [16] (σ_F, %)	.60	.60	2.5	.60	.35
Beamstrahlung parameter Υ	.440	.111	.075	.015	.010

The five designs in Table 1 are arranged in order of decreasing beamstrahlung parameter Υ. It is no accident that at least within a class (compare designs 1 and 2, or 3 and 4), reducing the beamstrahlung parameter (and, as we shall see, the average radiative energy loss) also reduces the luminosity : all the machine parameters (a much larger set than the restricted list quoted here) are deeply interdependent. One cannot arbitrarily attempt to improve the luminosity by increasing the pulse rate or the current, without destroying the technical self-consistency of the design. For instance, the product $f_{rep} \cdot k_b \cdot N$ of the pulse rate by the total current per pulse is limited by the affordable beam power: increasing the repetition rate is therefore impractical for fiscal reasons. It is not possible either to increase the individual bunch currents without affecting (among other things) all of the following: damping ring design, longitudinal wakefields in the Linac and hence energy spread, transverse wakefields that feed into emittance blowup and beam instabilities, not to mention the beamstrahlung flux itself. Reducing the IP spot sizes requires even more challenging emittances, is limited by quadrupole gradients achievable with present day rare earth magnet technology, and again increases the amount of beamstrahlung. Similarly, the Linac energy spread results from a delicate compromise between bunch current, bunch length (also related to beamstrahlung), RF frequency and available RF voltage, longitudinal and transverse wakefields, etc. [9] In that sense, our table represents designs that are technologically self-consistent to the extent possible, and optimized for luminosity and beamstrahlung at a given cost in electrical power.

4 e^+e^- and Photon-Photon Luminosity Spectra

We are now in the position to combine the calculation tools sketched in section 2 with collider design parameters, and predict the dependence of the luminosity on the effective e^+e^- or $\gamma\gamma$ c.m. energy. Beamstrahlung, however, is not the only phenomenon affecting the electron energy spectrum. First, the incident e^+ and e^- beams exhibit, before collision, a finite energy spread, as illustrated in Table 1. Second, electron initial state radiation

constitutes an irreducible source of electron energy loss which is at least as important as beamstrahlung in all designs except Design 1. The effect of initial state radiation on the electron energy spectrum is calculated using the electron energy distribution of Fadin and Kuraev [17] :

$$D_e(z,s) = \frac{1}{2}\beta(1-z)^{\frac{\beta}{2}-1}(1+\frac{3}{8}\beta) - \frac{1}{4}\beta(1+z) \quad , \tag{34}$$

where

$$\beta \equiv \frac{2\alpha}{\pi}(\log\frac{s}{m^2} - 1) \quad , \tag{35}$$

$\sqrt{s}$ is the center–of–mass energy of the interacting e^+ and e^-, and z is the fractional e^+ or e^- energy following initial state radiation. The distribution $D_e(z,s)$ is the leading term of the solution of an evolution equation which describes multiple collinear photon radiation to all orders in α. Note that $\sqrt{s}$ may be less than the nominal center–of–mass energy $\sqrt{s_0} = 2E_0$ if either the e^+ or e^- has radiated a significant amount of beamstrahlung photon energy, or $\sqrt{s}$ may be greater than $\sqrt{s_0}$ due to the intrinsic energy spread of the beams before collision.

When calculating the contribution of initial state radiation to the $\gamma\gamma$ luminosity we use the Weizsäcker–Williams single photon distribution $D_\gamma(\omega,x)$ defined by [18]

$$D_\gamma(\omega,x) = \frac{\eta(x)}{\omega}(1+(1-\omega)^2) \quad , \tag{36}$$

where

$$\eta(x) \equiv \frac{\alpha}{\pi}\log\frac{xE_0}{m} \tag{37}$$

and ω is the fractional Weizsäcker–Williams photon energy

$$\omega \equiv \frac{E_\gamma}{xE_0} \quad . \tag{38}$$

To add Weizsäcker–Williams photons to the photon flux we add $\Omega(y,t)$ to Eq.(17) or Eq.(21) where

$$\Omega(y,t) \equiv \int_y^1 D_\gamma(\omega,\frac{y}{\omega})\psi(\frac{y}{\omega},t)\frac{d\omega}{\omega} \quad . \tag{39}$$

In the remainder of this section, we calculate realistic e^+e^- and $\gamma\gamma$ energy and luminosity spectra, in the presence of beamstrahlung, intrinsic Linac energy spread, and initial state radiation, for the various Linear Collider designs considered above. To this effect, we incorporate the formalism presented in section 2, together with a naive model of the intrinsic energy spread [16] and the QED initial state radiation effects described above, into a Monte Carlo program. For a given set of IP parameters, this code supplies the user with the electron (respectively the photon) energy spectrum, and with the corresponding differential luminosity function as a function of the effective e^+e^- (respectively $\gamma\gamma$) center-of-mass energy. These spectra can be optionally weighted by the (energy-dependent) cross-section of the particle physics process under study.

Let us first examine individual particle spectra, the main characteristics of which are summarized in Table 2. Here we neglect Linac energy spread and initial state radiation

Table 2: Effect of beamstrahlung alone on e^- and γ energy spectra

Design Class	1 Palmer G	2 Palmer F	3 D-D wide bd	4 D-D nrrw bd	5 TESLA nrrw bd
Beamstrahlung parameter Υ	.440	.111	.075	.015	.010
Mean e^- energy loss (%)	17	2.3	4.3	0.5	0.4
R.M.S. e^- energy spread (%)	17	5.2	6.1	1.1	0.9
Number of radiated γ's/e^-	1.5	.46	1.2	.60	.76
Mean γ energy (%)	11	4.9	3.7	0.9	0.6
R.M.S. γ energy spread (%)	13	6.3	4.7	1.2	0.8

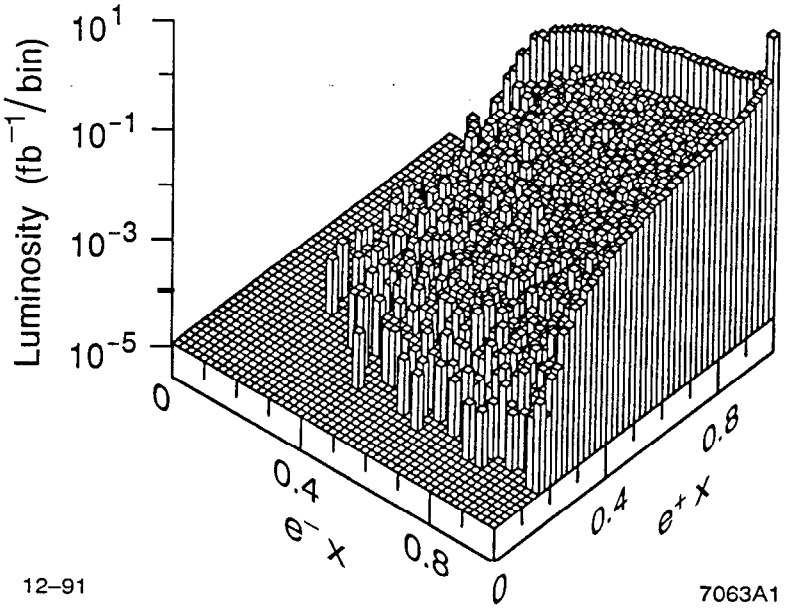

Figure 1: e^+e^- luminosity spectrum as a function of the fractional electron energy (e^- x) and the fractional positron energy (e^+ x), for the strong beamstrahlung X-band design (design 1). Linac energy spread is neglected. The total luminosity is 10 fb^{-1}. The bin size is .02 × .02.

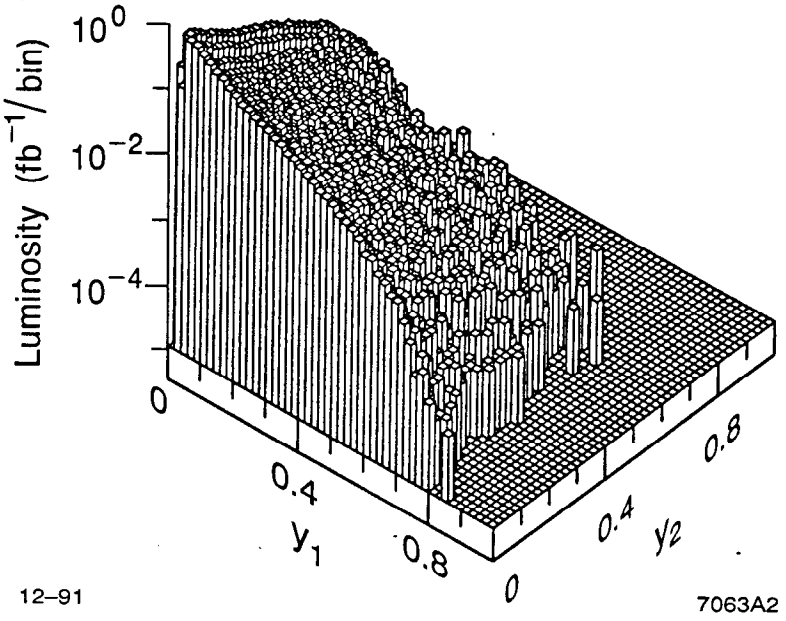

Figure 2: $\gamma\gamma$ luminosity spectrum as a function of the fractional photon energies y_1 and y_2, with a minimum $\gamma\gamma$ center-of-mass energy of 10 GeV. The figure corresponds to accelerator Design 1. Only the luminosity due to the collisions of beamstrahlung photons is shown. Luminosity from the collisions of two virtual (Weizsäcker–Williams) photons or of beamstrahlung photons with virtual photons is not included. The total e^+e^- luminosity is 10 fb^{-1}. The bin size is $.02 \times .02$.

to concentrate on beamstrahlung effects. All of the quantities shown in Table 2, with the exception of Υ, are e^+e^- luminosity-weighted. This implies, for example, that the mean electron energy loss quoted in Table 2 is smaller than the mean energy loss of an electron that has completed its journey through the opposing positron bunch. Fig. 1 displays, for the design with the highest beamstrahlung flux, the distribution of electron energies (normalized to the nominal beam energy E_0), vs the corresponding positron energy. For most events, only either the electron, or the positron, actually radiates a significant amount of energy, as evidenced by the edge bands. Fig. 2 contains the corresponding plot for the photon energies.

Let us now turn to the actual luminosity spectra for e^+e^- collisions. We display separately the dependence of beamstrahlung on the linear collider design (Fig. 3), and the relative importance, for two extreme cases of strong and quasi-classical beamstrahlung, of the three electron energy loss mechanisms (Fig. 4). Some of the salient features of the effective e^+e^- energy distributions are summarized in Table 3: the average c.m. energy

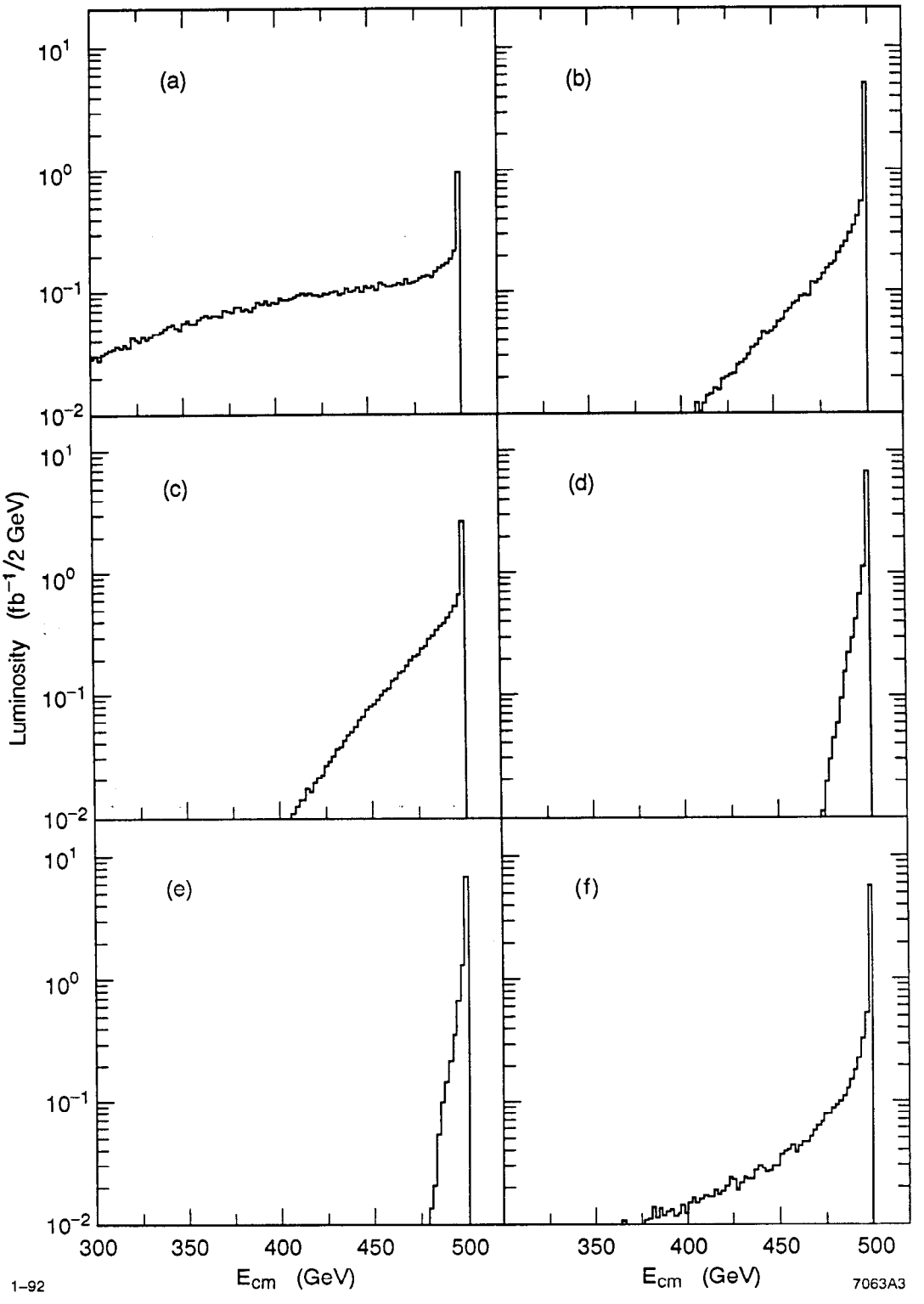

Figure 3: e^+e^- luminosity spectra in the presence of beamstrahlung, but neglecting Linac energy spread and initial state radiation, for various Linear Collider designs: (a) Palmer G; (b) Palmer F; (c) Desy-Darmstadt, wide band; (d) Desy-Darmstadt, narrow band; (e) TESLA. Curve (f) is the e^+e^- luminosity spectrum in the presence of initial state radiation, but neglecting Linac energy spread and beamstrahlung. All curves are normalized to a total e^+e^- luminosity of 10 fb^{-1}.

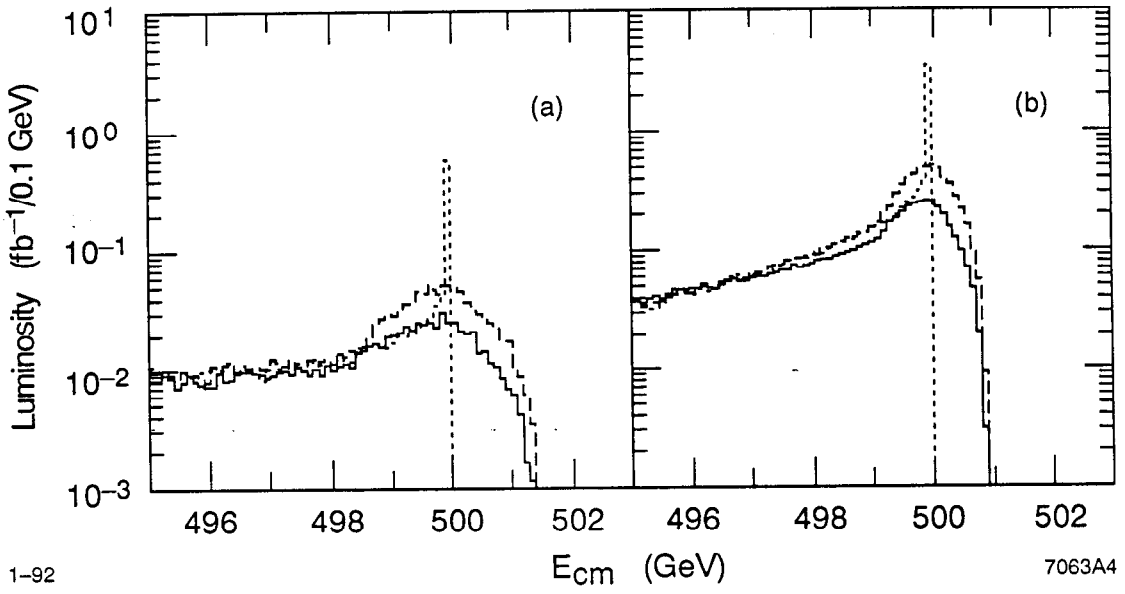

Figure 4: e^+e^- luminosity spectra in the presence of beamstrahlung only (dotted), of beamstrahlung and Linac energy spread (dashed), and of beamstrahlung, Linac energy spread, and initial state radiation (solid), for very different Linear Collider designs: a) X-band, strong beamstrahlung (Palmer G); b) TESLA. For each curve the total e^+e^- luminosity is 10 fb^{-1}.

Table 3: Effect of beamstrahlung, Linac energy spread, and initial state radiation on e^+e^- luminosity spectra

Design Class	1 Palmer G	2 Palmer F	3 D-D wide bd	4 D-D nrrw bd	5 TESLA nrrw bd
Beamstrahlung alone:					
Mean e^+e^- c.m. energy loss (%)	18	2	4	0.6	0.5
R.M.S. e^+e^- c.m. energy spread (%)	14	4	5	0.9	0.7
$\mathcal{L}$ within 0.5 GeV of E^0_{cm} (%)	6	45	15	47	43
$\mathcal{L}$ within 2.5 GeV of E^0_{cm} (%)	8	54	24	68	69
Linac Energy Spread Alone:					
Mean e^+e^- c.m. energy loss (%)	0	0	0	0	0
R.M.S. e^+e^- c.m. energy spread (%)	0.1	0.1	0.5	0.1	0.1
$\mathcal{L}$ within 0.5 GeV of E^0_{cm} (%)	56	56	15	56	82
$\mathcal{L}$ within 2.5 GeV of E^0_{cm} (%)	100	100	63	100	100
Initial State Radiation Alone:					
Mean e^+e^- c.m. energy loss (%)	5	5	5	5	5
R.M.S. e^+e^- c.m. energy spread (%)	11	11	11	11	11
$\mathcal{L}$ within 0.5 GeV of E^0_{cm} (%)	50	50	50	50	50
$\mathcal{L}$ within 2.5 GeV of E^0_{cm} (%)	61	61	61	61	61
Linac Energy Spread, Beamstrahlung, and Initial State Radiation:					
Mean e^+e^- c.m. energy loss (%)	22	7	9	5	5
R.M.S. e^+e^- c.m. energy spread (%)	17	12	12	11	11
$\mathcal{L}$ within 0.5 GeV of E^0_{cm} (%)	2	14	2	16	18
$\mathcal{L}$ within 2.5 GeV of E^0_{cm} (%)	5	32	11	40	40

Table 4: Effect of beamstrahlung and initial state radiation on the $\gamma\gamma$ luminosity spectra for $\gamma\gamma$ center-of-mass energies greater than 0.5 GeV

Design Class	1 Palmer G	2 Palmer F	3 D-D wide bd	4 D-D nrrw bd	5 TESLA nrrw bd
Beamstrahlung alone:					
Mean $\gamma\gamma$ c.m. energy (GeV)	29	14	10	3	2
R.M.S. $\gamma\gamma$ energy spread (%)	37	18	13	3	2
Lumi. enhancement $\mathcal{L}_{\gamma\gamma}/\mathcal{L}_{ee}$:	2.3	0.2	1.3	0.3	0.4
Beamstrahlung and Initial State Radiation:					
Mean $\gamma\gamma$ c.m. energy (GeV)	26	16	13	10	8
R.M.S. $\gamma\gamma$ energy spread (%)	37	29	21	22	20
Lumi. enhancement $\mathcal{L}_{\gamma\gamma}/\mathcal{L}_{ee}$:	3.7	0.8	2.3	0.9	1.0

loss, the effective c.m. energy spread, and the fraction of the luminosity produced within a given energy interval of the nominal c.m. energy. For this last variable, we consider both a very narrow energy window (0.5 GeV), comparable to the r.m.s intrinsic Linac energy spread, and a relatively wide one (2.5 GeV), comparable to the total width of the top threshold excitation curve. The effects of beamstrahlung, Linac energy spread and initial state radiation are again first evaluated separately, and then combined.

Inspection of the luminosity spectra warrants the following observations: Design 1, the strong beamstrahlung X-band design ("Palmer G") [19], has a moderate horizontal/vertical beam aspect ratio (25:1), ensuring high luminosity, but at the cost of intense beamstrahlung. Only a few % of the luminosity falls within a reasonably narrow energy band. Linac energy spread plays a negligible role in this case. Design 2, a moderate beamstrahlung X-band design ("Palmer F"), has IP parameters which are identical to the "Palmer G" design, except that the beams have been considerably flattened (180:1 aspect ratio) to reduce the radiated energy, at the cost of a factor of 4 in luminosity. In this design, the moderate intrinsic Linac energy spread is typical of what the authors consider routinely achievable with longitudinal wakefield compensation [20]. Its contribution to the dilution of the spectrum is comparable, for very narrow structures, to that of beamstrahlung. Design 3, the Desy-Darmstadt wide band design [21], achieves the required luminosity by trading single bunch current for a large number of low current bunches, yielding a beamstrahlung spectrum intermediate between the X-band designs. But the large Linac energy spread (which results from the lack of longitudinal wakefield compensation, and is not an intrinsic property of this design class), completely dominates the spectrum shape near the maximum energy. Design 4 is the Desy-Darmstadt narrow band design [14]. Its accelerator technology, design philosophy and aspect ratio are the same as in the previous design, but beamstrahlung has been reduced (again at a sizeable cost in luminosity) by increasing both transverse and longitudinal IP spot dimensions within

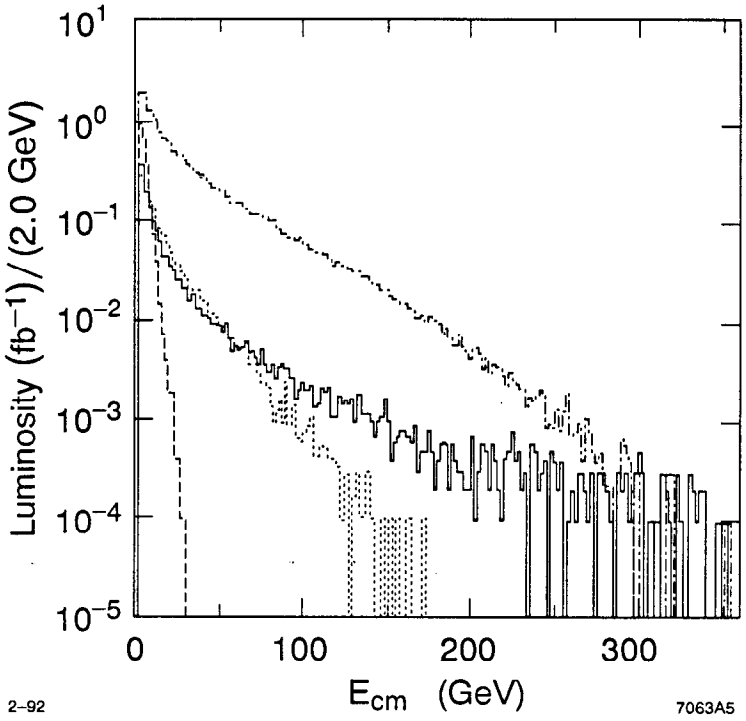

Figure 5: $\gamma\gamma$ luminosity spectra for $\gamma\gamma$ center-of-mass energies greater than 2 GeV. The solid curve is the luminosity from the collisions of virtual (Weizsäcker–Williams) photons only. The remaining curves are the luminosity spectra from the collisions of beamstrahlung photons only, for various Linear Collider designs: X-band, strong beamstrahlung (Palmer G) is dot–dashed; X-band, moderate beamstrahlung (Palmer F) is dotted; TESLA is dashed. All curves are normalized to a total e^+e^- luminosity of 10 fb^{-1}.

constraints imposed by the Linac and injection complex. The beamstrahlung spectrum now looks very similar to that achieved by the TESLA narrow band design. The intrinsic Linac energy spread is minimized by the combination of a relatively long bunch and of careful compensation of the longitudinal wakefield by the curvature of the RF waveform; it no longer dominates the resolving power for very narrow structures. Design 5 is TESLA, narrow band [22]. Thanks to the very long bunches and large spot sizes, beamstrahlung occurs here in the almost classical regime. Combined with an extremely narrow Linac energy spread (which assumes very careful compensation [23]), it appears to provide (at least so far and if its technology holds its promises) the most precise tool for top threshold studies.

Finally, we consider briefly the photon-photon luminosity potential of e^+e^- linear colliders. The c.m. energy signature of the five designs we considered is summarized in Table 4 and the luminosity spectra for three of those designs is displayed in Fig. 5. The average $\gamma\gamma$ c.m. energy varies over a wide range, with a very large fractional spread; and the luminosity enhancement due to multiphoton emission mostly affects, as expected, the softest part of the spectrum. Clearly, only for the high Υ, X-band design does beamstrahlung extend the potential for two-photon physics beyond what is naturally accessible with initial state radiation photons.

5 Summary

We evaluated the effective e^+e^- and $\gamma\gamma$ luminosity spectra for several classes of Linear Collider designs, in the presence of multiphoton beamstrahlung, initial state radiation, and Linac energy spread. At the high energy end, the shape of the e^+e^- c.m. energy distribution depends not only on the beamstrahlung power spectrum, but also on the achievable Linac energy spread, both of which vary considerably from one set of accelerator parameters to the other. For the low-beamstrahlung, narrow-band designs we considered, the low-energy tail of the e^+e^- luminosity spectrum is dominated by initial state radiation rather than by beamstrahlung. Beamstrahlung, however, is an important component of the low energy tails of the other designs; in fact, beamstrahlung dominates the low energy tail of the high Υ, X-band design. Initial state radiation also dictates the shape, and the kinematic reach, of the effective $\gamma\gamma$ c.m. energy distribution in all cases except that of the high Υ, X-band design.

Acknowledgements

This work was supported in part by U.S. Department of Energy contract DE-AC03-76SF00515. One of us (W.K.) also wishes to thank the Max-Planck-Institut fur Physik in Munich (Germany) for its warm hospitality during the initial stage of this research.

References

[1] M. Bell and J. S. Bell, *Part. Accl.* 24, 1 (1988);

R. Blankenbecler and S. D. Drell, *Phys. Rev. Lett.* 61, 2324 (1988);
P. Chen and K. Yokoya, *Phys. Rev. Lett.* 61, 1101 (1988);
M. Jacob and T. T. Wu, *Nucl. Phys.* B303, 389 (1988);
V. N. Baier, V. M. Katkov, and V. M. Strakhovenko, Institute of Nuclear Physics Preprint 88–168 (1988), Novosibirsk;
and references therein.

[2] A. A. Sokolov and I. M. Ternov, *Radiation from Relativistic Electrons*, AIP Trans. Series, 1986.

[3] R. Blankenbecler and S. D. Drell, Phys. Rev. Lett. 61, 2324 (1988).

[4] K. Yokoya and P. Chen, Proc. IEEE Part. Accel. Conf. 89CH2669-0, 1438 (1989).

[5] P. Chen, *Differential Luminosity under Multiphoton Beamstrahlung*, SLAC-PUB-5615, 1991; submitted to Phys. Rev. D.

[6] P. Chen and K. Yokoya, *Phys. Rev.* **D38**, 987 (1988).

[7] P. Chen, in *High Energy Physics in the 1990's, Snowmass 1988*, World Scientific, 1989;
P. Chen and V. L. Telnov, Phys. Rev. Lett., 63, 1796 (1989);
R. Blankenbecler, S. D. Drell, and N. Kroll, Phys. Rev. D40, 2462 (1989);
M. Jacob and T. T. Wu, Nucl. Phys. B327, 285 (1989).

[8] For a review, see, for example, K. Yokoya and P Chen, *Beam-Beam Phenomena in Linear Colliders*, Lecture given at the US-CERN Accelerator School, Hilton Head, SC, 1990; KEK-Preprint-91-2, 1991..

[9] R.B. Palmer, Prospects for High-Energy e^+e^- Linear Colliders, Ann.Rev.Nucl.Part.Sci.40:529-592,1990.

[10] W.A. Barletta, D.L. Burke, P. Chen, S. D. Ecklund, V. Granatstein, John Irwin, W. Kozanecki, H.G. Moser, R.B. Palmer, J.M. Paterson, R.D. Ruth, A W. Schnell, J. Seeman, R. Shafer, P.B. Wilson, Linear Colliders. SLAC-PUB-5597 (1991), and Proceedings of the 1990 DPF Summer Study on High-Energy Physics: Research Directions for the Decade, Snowmass, Co.

[11] We should actually mention also the Clic approach, which relies on the very different philosophy of a high current, low energy superconducting drive Linac feeding RF to the high energy, low current main Linac. This technology primarily aims at achieving c.m. energies well in excess of 1 TeV, somewhat beyond the scope of the present workshop. From the narrow viewpoint of the effective c.m. energy distribution, Clic is not fundamentally different from the strong beamstrahlung design considered in this paper. This last comment also applies to the X-band Novosibirsk/Serpukhov design. See, respectively, W. Schnell, Proceedings of the Workshop on Physics with Linear Colliders, Saariselka, Finland, Sept. 9-14, 1991; and V. Balakin, ibid.

[12] B. Richter, Proceedings of the Workshop on Physics with Linear Colliders, Saariselka, Finland, Sept. 9-14, 1991; R. Ruth, ibid.

[13] G.-A. Voss, Proceedings of the Workshop on Physics with Linear Colliders, Saariselka, Finland, Sept. 9-14, 1991.

[14] T. Weiland, Status Report of a 500 GeV S-Band Linear Collider Study, Proceedings of the Workshop on Physics with Linear Colliders, Saariselka, Finland, Sept. 9-14, 1991.

[15] M. Tigner, Proceedings of the Workshop on Physics with Linear Colliders, Saariselka, Finland, Sept. 9-14, 1991; B. Wiik, ibid.

[16] The Linac energy spectrum (for each beam separately) can be approximated by a uniform distribution, centered on the nominal energy, and of full fractional width σ_F. For designs 1,2, and 5, the authors actually quote an r.m.s. width σ_R which we translated using the trivial relationship $\sigma_F = \sqrt{12}\ \sigma_R$; for designs 3-4, the authors quote σ_F in the energy of those particles contained within a longitudinal interval of $\pm 2\sigma_z$.

[17] E.A. Kuraev and V.S Fadin, *Sov. J. Nucl. Phys.* **41**, 466 (1985).

[18] V.M. Budnev et al., *Phys. Rep.* **15**, 181 (1975).

[19] The notations "Palmer F" or "Palmer G" refer to version F or G, respectively, of a Linear Collider design as presented in ref. [9].

[20] K. Bane, private communication.

[21] G.-A. Voss, presentation to the Ringberg Workshop on High Precision vs High Luminosity in e^+e^- Physics, Ringberg, Germany, April 1991 (unpublished).

[22] B. Wiik, talk presented at MPI Munich, Feb. 91 (unpublished).

[23] D. Rubin, private communication.